Plume-driven subduction termination in 3-D mantle convection models

Erin Heilman[1,2] **and Thorsten W. Becker**[1,2,3]

[1]Institute for Geophysics, Jackson School of Geosciences, The University of Texas at Austin, Austin TX, USA

[2]Department of Earth and Planetary Sciences, Jackson School of Geosciences, The University of Texas at Austin, Austin TX, USA

[3]Oden Institute for Computational Sciences, The University of Texas at Austin, Austin TX, USA

Key Points:

- mantle plumes can terminate subduction in 3-D, damage rheology convection
- plumes can modulate subducting slabs and plate tectonic regimes
- plume-slab interactions are plausible contributions to the Karoo-Gondwana event

Corresponding author: Erin Heilman, `eheilman@lanl.gov`

In press at G-Cubed, June 2024.

Abstract

The effect of mantle plumes is secondary to that of subducting slabs for modern plate tectonics when considering plate driving forces. However, the impact of plumes on tectonics and planetary surface evolution may nonetheless have been significant. We use numerical mantle convection models in a 3-D spherical chunk geometry with damage rheology to study some of the dynamics of plume-slab interactions. Substantiating our earlier 2-D results, we observe a range of interaction scenarios, and that the plume-driven subduction terminations we had identified earlier persist in more realistic convective flow. We analyze the dynamics of plume affected subduction, including in terms of their geometry, frequency, and the overall effect of plumes on surface dynamics as a function of the fraction of internal to bottom heating. Some versions of such plume-slab interplay may be relevant for geologic events, e.g. for the inferred ∼183 Ma Karoo large igneous province formation and associated slab disruption. More recent examples may include the impingement of the Afar plume underneath Africa leading to disruption of the Hellenic slab, and the current complex structure imaged for the subduction of the Nazca plate under South America. Our results imply that plumes may play a significant role not just in kick-starting plate tectonics, but also in major modifications of slab-driven plate motions, including for the present-day mantle.

Plain Language Summary

Subduction of cold, strong lithospheric slabs is the main plate driving force within mantle convection. However, hot upwellings, mantle plumes, may have a greater role in modulating plate motions and slab trajectories than previously thought. We use 3-D numerical convection models that account for the weakening of rocks due to the accumulation of deformation to understand the effect that mantle plumes can have on subduction zones. We show that plumes can terminate subduction in a range of circumstances. We also test the effect of the amount of internal heating compared to heat from the core which is the major convective control on the importance of plumes. We discuss cases where these plume-slab terminations may have occurred on Earth, in the geological past, and for the present day through plate reconstructions and consideration of seismic tomography.

1 Introduction

Subduction of the cold, lithospheric boundary layer is the main driving force of plate tectonics through slab pull due to temperature-dependent viscosity and the dominance of internal heating in mantle convection. However, there is also feedback between subducting slabs and mantle plumes as long as there is some degree of bottom heating (e.g. Davies, 1986; Zhong, 2006; Leng & Zhong, 2008). While instabilities of the bottom thermal boundary layer can lead to plume sources anywhere, a perturbation, for instance due to a subducting slab, will affect the timing and location for the formation of mantle plumes (e.g. Tan et al., 2002; Hassan et al., 2015; Li & Zhong, 2017; Dannberg & Gassmöller, 2018; Arnould et al., 2020). This is one example of the possible feedback, or "talk-back", between plumes and slabs.

When mantle plumes reach the lithosphere, they too can perturb the top thermal boundary layer, e.g. creating hotspot volcanics and large igneous provinces (LIPs), contributing to rifting and supercontinental breakup, subduction initiation, as well as sustaining a low viscosity asthenosphere below (e.g. Jellinek & Manga, 2004; Koppers et al., 2021). When plumes reach the lithosphere in the vicinity of a subduction zone they can interact with slabs by temporarily speeding up plates (van Hinsbergen et al., 2011; Pusok & Stegman, 2020), affecting trench motion and convergence rates (Betts et al., 2012; Mériaux et al., 2015), get deflected by slabs (Druken et al., 2014; Kincaid et al., 2013), or lead to slab disruption (Liu & Stegman, 2012; Heilman & Becker, 2022).

Such plume-slab disruption has been less well explored because one may expect a strong, thick slab to survive any plume-induced deformation. As a consequence, when discussing plume-slab interactions, most think of plumes as a possible driver to initiate subduction, and plume-affected plate tectonics has been explored in several models. Plumes may kick-start subduction either directly or by means of emplacing surface density contrasts (Ueda et al., 2008; Rey et al., 2014; Gerya et al., 2015; Baes et al., 2020), and plume induced modification of plate speeds may also lead to far field forces for subduction initiation (van Hinsbergen et al., 2021).

However, if strain-dependent damage rheologies are accounted for, plumes do in fact appear capable of terminating subduction as well (Heilman & Becker, 2022). This process can be associated with an interesting feedback loop: Flow induced by a subducting slab may initiate a mantle plume at the core–mantle boundary, affect its conduit,

and that plume may then in turn terminate subduction close to the surface after its ascent through the mantle. Subsequently, the broken-off slab descends through the mantle, to possibly start the cycle anew when reaching the bottom, re-seeding a plume, which may then re-initiate subduction at the surface.

While this cycle would, of course, be simply one aspect of the time-dependent mantle convection system which can include episodic or irregular plate motions, it is one interaction loop that leaves possibly diagnostic traces in the rock record. For example, Fletcher and Wyman (2015) identified that in the past 60 Ma, 18 plumes have been within 1000 km of subduction zones, which points to plume-slab interactions, and potential terminations, as a relevant process to consider for the evolution of the plate tectonic system. Heilman and Becker (2022) explored the effects of internal heating, and thickness, or average temperature/age, of slabs as controlling factors for the likelihood of plumes terminating slabs and modifying the overall tectonic regime, such as a transition from plate-tectonics to stagnant lid. However, our earlier work was limited to 2-D, and one may rightly ask if such a restriction of flow is a precondition for plume-slab termination.

Investigating the nature of plume-slab termination in 3-D is both more realistic and more challenging. For the present-day mantle, we appear to mainly see plume-slab interactions where plumes are taking advantage of existing slab windows or tears, formed by plate reorganizations or local slab dynamics (Obrebski et al., 2010; Betts et al., 2012; Portner et al., 2017, 2020). Previously, Betts et al. (2012) showed based on 3-D modeling that a plume could modulate subduction in the case of trench rollback causing a subducting slab to move over a plume head. In this instance, a slab window was formed and subduction continued once the slab rolled completely over the plume head.

Investigations of suggested recent plume advance include the case of Canary toward the Alboran slab underneath the Atlas mountains (Duggen et al., 2009; Sun et al., 2014; Mériaux et al., 2015) and Afar toward Anatolia and the Hellenic subduction zone (Ershov & Nikishin, 2004; Faccenna et al., 2013; Hua et al., 2023). Present-day settings include the Yellowstone/Farallon case (Obrebski et al., 2010; Liu & Stegman, 2012) and the South American Juan de Fuca plume-slab window (Portner et al., 2017, 2020). These studies point to the lithosphere, e.g. in terms of slab tears or windows during trench rollback, or delamination, being the dominant control, and mantle plumes mainly responding to lithosphere dynamics. Plume-driven slab termination in 3-D will depend on the

lateral extents necessary for the interaction to cover, and thermo-mechanical heterogeneity of the mantle and crust. In particular, subduction termination may become more relevant when damage rheologies or other tectonic inheritance leads to weakening of slabs, including by segmentation and tears, or heterogeneous lithosphere with preserved zones of weakness (van Hunen & van den Berg, 2008; Betts et al., 2012; Fuchs & Becker, 2019; Gerya et al., 2021).

Here, we model 3-D, mantle convection in a spherical "chunk" geometry with damage rheology and a mixed heating regime similar to Earth's convective vigor. We explore how damage rheology affects plume-slab interactions and show that plume-induced slab termination is indeed possible in 3-D. We discuss possible instances where this may have happened from the geologic record and present-day seismic tomography to relate our numerical models to the Earth.

2 Model Setup

We model mantle convection as a fluid problem in the infinite Prandtl number and incompressible, Boussinesq approximation. Conservation of momentum and mass are then given by

$$-\nabla \cdot [2\eta\varepsilon(\mathbf{u})] + \nabla p = \rho\mathbf{g} = \rho_0\alpha(T - T_0) \tag{1}$$

$$\nabla \cdot \mathbf{u} = 0, \tag{2}$$

and conservation of energy without shear heating by

$$\rho C_p \left(\frac{\partial T}{\partial t} + \mathbf{u} \cdot \nabla T\right) - \nabla \cdot k\nabla T = \rho H, \tag{3}$$

while allowing for advection of a compositional or general tracer field c

$$\frac{\partial c}{\partial t} + \mathbf{u} \cdot c = 0. \tag{4}$$

Here, ε is the strain-rate tensor, $\mathbf{u}$ velocity, p pressure, g gravity, T temperature, ρ density, with a reference of ρ_0 at T_0, C_p specific heat capacity, k thermal conductivity, H the internal heat production, η viscosity, α thermal expansivity, and c composition. Eqs. (1) and (2) capture laminar Stokes flow, driven by thermal body forces, and eq. (3) describes the temperature field that is diffused and advected with the flow velocity $\mathbf{u}$, where the right-hand term is internal heat production. Eq. (4) governs how diffusion-free compositional fields evolve over time; in our models the compositional field tracked is a pas-

sive, effective "strain" property used to approximate damage evolution, as in Fuchs and Becker (2019, 2021), and does not involve additional, e.g., density contributions.

To solve eqs. (1-4), we use the open-source, finite element code *ASPECT* (Kronbichler et al., 2012; Heister et al., 2017; Fraters et al., 2019). Our approach overall follows that of Heilman and Becker (2022), but we employ a Newtonian, Frank-Kamenetskii linearized temperature-dependent viscosity law (cf. Tackley, 2000a; Stein & Hansen, 2013) to simplify the model. The temperature-dependent part of viscosity is given by

$$\eta\left(T\right) = \eta_{\mathrm{ref}} \exp\left[\frac{E}{1+\frac{T}{T_{\mathrm{ref}}}} - \frac{E}{2}\right] \tag{5}$$

where η_{ref} is a reference viscosity, E is a non-dimensional activation energy, and T_{ref} is the reference temperature for viscosity. Added into this viscosity law is a viscosity jump at 660 km depth, where the η_{ref} is increased by a factor of 30 in the lower mantle, as expected from geoid modeling and slab sinking rates (e.g. Hager, 1984; Ricard et al., 1993; Steinberger & Calderwood, 2006).

Additionally, we include visco-plasticity and a simplified damage rheology in our models (e.g. Tackley, 2000b; Ogawa, 2003; Auth et al., 2003; Fuchs & Becker, 2019). *ASPECT* employs plasticity and a possible strain-weakening for modulating the yield stress (Glerum et al., 2018). When the viscous stress ($2\eta\dot{\varepsilon}_{II}$) exceeds the yield stress the viscosity is rescaled back to an effective yield viscosity (e.g., Moresi & Solomatov, 1998; Enns et al., 2005).

$$\eta_{eff} = \frac{\sigma_y}{2\dot{\varepsilon}_{II}}. \tag{6}$$

We then use a strain-based damage variable γ to reduce the yield stress from the background value (e.g. Lavier et al., 2000; Ogawa, 2003). Damage, γ, evolves according to

$$\frac{d\gamma}{dt} = \dot{\varepsilon}_{II} - \gamma\ A_d \exp\left[E_\gamma\left(T - T_{\mathrm{ref}}\right)\right] \tag{7}$$

where $\dot{\varepsilon}_{II}$ is the second invariant of the strain-rate tensor, A_d is a timescale for strain-healing, and E_γ another non-dimensional activation energy, allowing for temperature- and time-dependent strain healing as in Fuchs and Becker (2019). Combining plasticity and such a damage rheology can approximate the behavior of micro-physical weakening processes like those inferred from grain-size dependent rheologies (Fuchs & Becker, 2021), which is one of the suggested mechanisms for strain localization in the lithosphere (e.g. Auth et al., 2003; Landuyt et al., 2008; Landuyt & Bercovici, 2009; Bercovici & Ri-

174 **Table 1.** Model parameters

Parameter	Value
Temperature difference between top and bottom bound. cond.	2500 K
Reference density ρ_0	3700 kg/m^3
Reference temperature T_0	1873 K
Thermal expansivity α	$2 \cdot 10^{-5}$ K^{-1}
Thermal diffusivity κ	10^{-6} m^2/s
Specific heat capacity C_p	750 J/gK
Internal heating rate H	$5.0 \cdot 10^{-12}$ W/kg
Minimum viscosity η_{min}	10^{18} Pas
Maximum viscosity η_{max}	$2.5 \cdot 10^{24}$ Pa s
Non-dimensional activation energy E	29.95
Reference viscosity η_{ref}	$4.5 \cdot 10^{19}$ Pa s
Reference temperature for viscosity T_{ref}	2500 K
Reference yield stress for Damage Model	140 MPa
Yield stress for No Damage Model	55 MPa
Non-dimensional strain weakening factor ϕ	0.25
Non-dimensional activation energy for strain healing E_γ	250
Non-dimensional timescale for strain healing A_d	10^{-7}

167 card, 2016). The strain-weakening factor ϕ is set to reduce the yield stress from the ref-
168 erence σ_y at $\gamma = 0$ linearly to $\phi\sigma_y$ at $\gamma \geq 5$; here, a 75% drop from 140 to 35 MPa
169 (Table 1), with parameters based on Heilman and Becker (2022). This damage evolu-
170 tion formulation allows plastically weakened regions to persist and be advected in cold
171 lithosphere while damage in the hotter mantle is healed more readily (cf. Fuchs & Becker,
172 2019, 2021). We also compare our damage rheology reference model to a model with-
173 out to explore the effect of damage on plume-slab interaction dynamics.

175 Our 3-D spherical "chunk" model is shown in Figure 1; at equivalent depths, its
176 surface area corresponds to that from latitude $-45°$to $45°$and longitude of $-50°$to $50°$on
177 Earth. Temperature boundary conditions for our mixed heating convection model are
178 273 K and 2573 K for the surface and core-mantle boundary (CMB), respectively, and

In press at G-Cubed, June 2024.

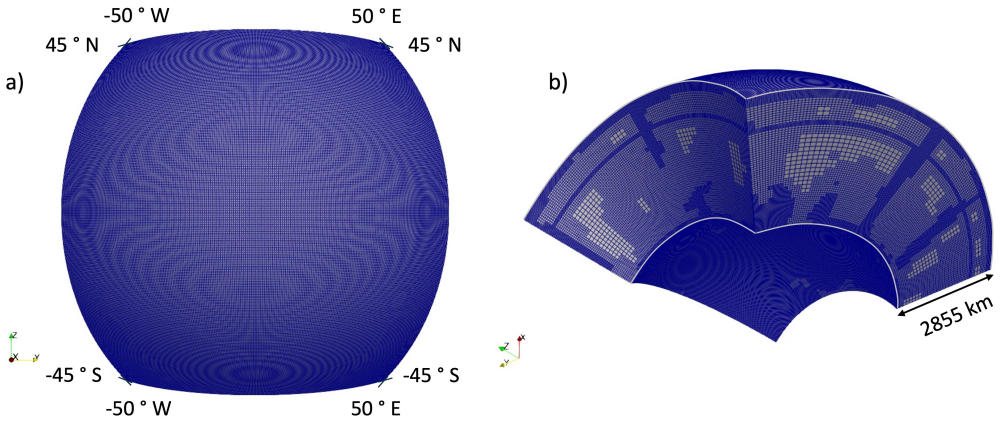

194 **Figure 1.** 3-D spherical "chunk" geometrical model domain, showing the surface extent in
195 terms of geographic coordinates (a), and in side view (b) with depth extent of the model (whole
196 mantle depths). b) also shows an example of adaptive and predefined mesh refinement, with
197 higher resolution in boundary layers and around evolving temperature/viscosity anomalies.

179 the mechanical boundary conditions are free slip on all sides. The model domain size was
180 chosen so as to allow convective structures with length scales several multiples of model
181 thickness (i.e., aspect ratios larger than unity) while minimizing computational cost. To-
182 gether with the reflective boundary conditions, we expect the model geometry to have
183 a moderate effect on convection, such as for slabs to have a bit more of a tendency to
184 get folded (e.g. Enns et al., 2005), and maximum plate scales to be lower than on Earth.

185 We use a reference internal heating value of $5 \cdot 10^{-12}$ W/kg (Table 1) and com-
186 pare models with different internal heating production rates. The balance of bottom to
187 internal heating is the major control on the relative importance of mantle plumes, from
188 a general understanding of convection (e.g. Davies, 1986; Zhong, 2006; Leng & Zhong,
189 2008; Foley & Becker, 2009) and our earlier, 2-D tests within the context of plume-slab
190 interactions as discussed here (Heilman & Becker, 2022). The Earth's ratio of internal
191 to bottom heating is only broadly constrained (e.g. Lay et al., 2008; Jaupart et al., 2015),
192 but expected to be time-variable over planetary history because of the decay of radio-
193 genic material, such that plume importance may have increased over time.

198 By specifying uniform CMB temperature boundary conditions, plumes freely rise
199 due to temperature instabilities, governed by dynamically consistent convection, at Earth-
200 like convective vigor. The effective Rayleigh number of our reference computation is $\sim$

$3.5{\cdot}10^6$. Bulk metrics such as surface heat flow are in Earth-like ranges (sec. 3.3), with surface velocities are ∼3 times lower than present-day plate speeds. We thus expect the dimensionalized model times to broadly correspond to actual time for our reference models. However, to make models with different parameters and hence convective vigor overall comparable, e.g., in terms of frequency of tectonic events, we also report times in units of overturn time, i.e. the typical time taken for a density anomaly to traverse the mantle and back. For the Earth, those can be converted by multiplying with relevant timescales, ∼300 Myr for ∼2 cm/yr average vertical motions. When comparing our reference model with a non-damage rheology case, we use a lower yield stress to roughly match the convective vigor between the models (cf. Fuchs & Becker, 2022).

3 Results

3.1 Damage Rheology Model

We first explore a model with damage rheology and a yield stress of 140 MPa (Figure 2) building on the work by Heilman and Becker (2022). Including damage rheology in a convection model leads to potential localization of deformation, formation of persistent weak zones (e.g. Auth et al., 2003; Ogawa, 2003; Landuyt et al., 2008; Fuchs & Becker, 2019), as well as possibly an overall drop in bulk lithospheric strength, e.g. if damage reduces the yield stress over time on average (cf. Foley & Bercovici, 2014; Fuchs & Becker, 2022). In our models, the damage rheology weakens the subducting slabs and allows the weakness to persist because the slabs are cold. When mantle plumes strike the lithosphere, damage can be reduced as the plumes introduce heat. This can lead to the healing effect to take over, reducing the associated inherited weak zones on the surface. This does not mean that plumes make the lithosphere strong in our models, they still tend to decrease the viscosity of the lithosphere that they underplate, and generally lead to some mode of extension on the surface.

The reference model was analyzed for a total of 3 model overturns, beginning from an initially dynamically steady-state model run. During the qualifying model run time of 3 overturns, we observe 7 instances of plume-slab termination of the kind we explored in 2-D (Heilman & Becker, 2022), i.e. an average of 2.3 terminations every overturn. Termination of subduction was determined from visual, temperature thresholding analysis when no part of the cold, downwelling structure below a temperature threshold typical

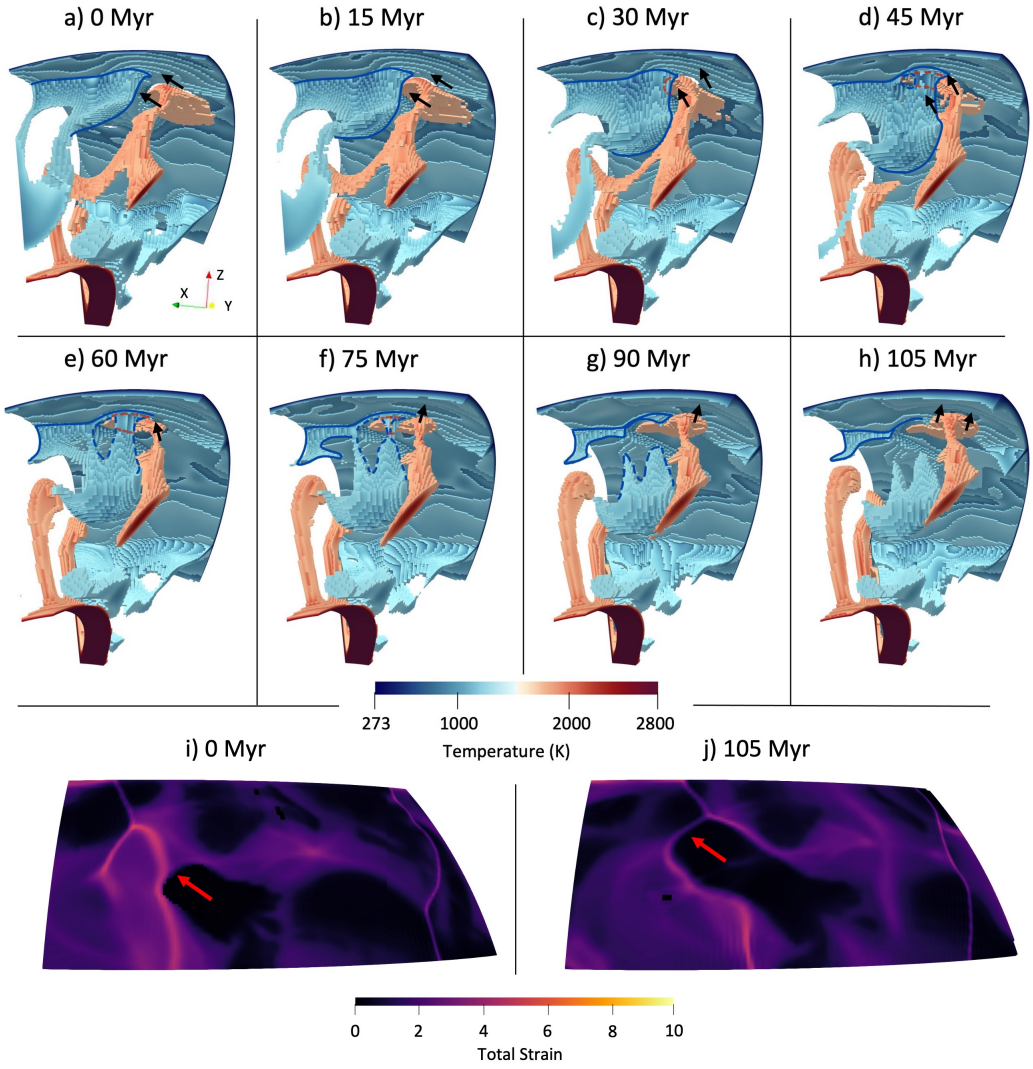

Figure 2. Example of a rising mantle plume terminating a subduction zone in 3-D for our reference model with damage. a-h show temperature thresholds of plumes (∼1750-2773 K, red colors) and slabs (273-∼1250 K, blue) during several times showing plume-slab interactions. Plots i-j show the damage, expressed as effective "strain", at the surface for the first (a and i) and last (h and j) time slice. When the plume strikes the surface, it resets the damage (black areas) and it influences the subduction zone (pink) to bend around it as shown by the red arrows tracking the plume's movement along with the lithosphere on the surface. See Figure **??** for an interpreted version.

of continuous subduction was connected to the surface anymore. Such plume-induced termination events do not tend to overlap in time; however, we do observe one instance when two termination sequences are present at overlapping times. Terminations are clustered in time, with periods of quiescence, similar to what was observed and analyzed by Heilman and Becker (2022).

Six of the seven termination events occurred by means of a single plume impinging on a subduction zone causing the termination. The six events do vary in where the plume interacts with the slab along its lateral extent. If the plume strikes the center of the subducting slab, the termination tends to develop by creating a hole in the slab that then grows and extends along the length of the slab until it is fully terminated (as in Figure 2). If the plume head interacts with the slab closer to the subducting slab's lateral extent, then the termination has an unzipping effect as the slab begins detaching at the plume head and continues along the length of the slab. The exceptional, 7^{th} termination was caused by two plumes on both sides of the subduction zone that pinched out the subducting slab to shut off subduction.

To visualize the plume-slab interactions and terminations we applied a temperature threshold for both the mantle plumes and subducting slabs. This thresholding allowed us to visualize features and interactions easily in 3-D (see Supplementary file S1). Figure 2a-h shows the temperature thresholding on the left for a typical plume-slab termination event with an interpretation of the dynamics of the typical termination. This view is a small section of the model focusing on a single interaction with the viewpoint in the mantle looking up towards the model surface. This interaction lasts for ∼105 Myr from initiation to cessation. The subducting slab is outlined in blue and the arrows indicate movement of the mantle plume. In panels a and b the mantle plume is sliding diagonally into the subduction zone from behind.

As the plume collides with the back of the slab the direction of the plume's movement changes to pushing almost perpendicular to the slab. In panel d we begin to see the plume breaking through the subducting slab due to the plume warming the subducting slab. With the plume pushing on the subducting slab, we see trench advance in the subduction zone. Trench advance is atypical during the reference model run for subduction zones that do not interact with plumes, indicating a particular mode of plume af-

fected dynamics. In some cases, the trench advance can lead to a period of flat slab subduction, as in Heilman and Becker (2022).

Panels e-g show the slab hole growing larger while the mantle plume continues to push against the slab. Once the slab detaches from the surface (panel g), the motion of the plume changes again as the slab is no longer impeding its ascend.

Figure 2i-j show the total accumulated strain of the surface (i.e. map view of the same area of a-h). Total accumulated strain here is the amount of damage in the model. Panel i shows the initial configuration of accumulated strain in the surface. The plume is represented by the red arrow and the subduction zone is the pink arc to the left of the red arrow. The plume head track in these images is black i.e. has no damage due to the heat in the plume effectively healing the damage in the lithosphere above it. As the plume terminates subduction, the damage that was accumulated in the subduction zone arc (the pink, curved region around the red arrow) in the lithosphere deflects around the plume head (panel j). This configuration of damage remains frozen in the lithosphere and is advected along the surface until a new subduction zone is initiated from the damaged arc (cf. Foley & Bercovici, 2014; Fuchs & Becker, 2019; Heilman & Becker, 2022).

We group the observed styles of termination into two figures each, showing first an interpretation of the dynamics and then showing the terminations in temperature, yield stress, strain rate, and total strain (accumulated damage) before and after termination, where termination is inferred from the visualization as the time when the slab is fully detached.

Figure 3 shows the termination in temperature, yield stress, strain rate, and total strain/damage fields. In the yield stress (c-d), we see that the subducting slab is fully weakened and the plume is strong due to its inherent higher temperature (cf. Fuchs & Becker, 2019). From this angle we can see that the surface of the model has areas of stronger and weaker lithosphere due to the damage present in the model. The strain rate (e-f) shows higher strain rates in the curved part of the slab close to the surface and in the mantle plume. The total strain (g-h) shows that the subducting slab has a value of accumulated strain of roughly 3 that increases slightly towards the bottom of the slab, which is due to the cool temperature of the slab slowing the rate of strain healing. The plume is not visible as it has an accumulated strain of zero due to its heat, which is shown here in black.

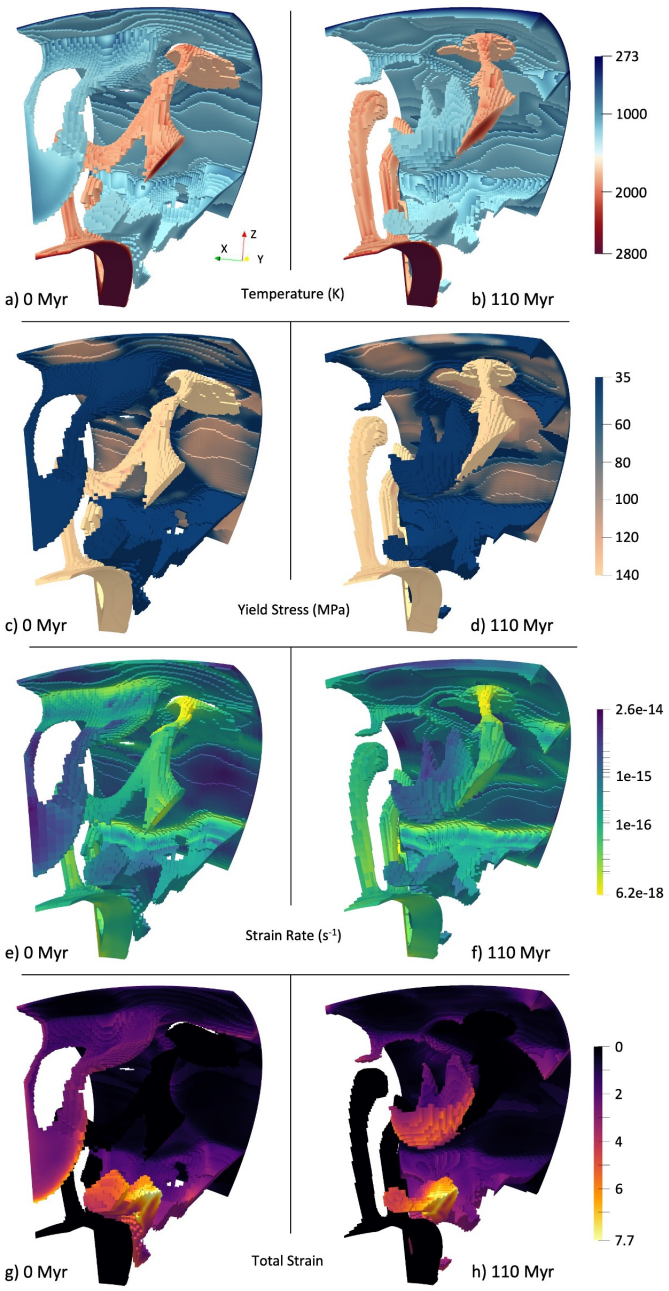

Figure 3. Temperature, yield stress, strain rate, and accumulated strain (damage) before (a, c, e, g) and after termination (b, d, f, h) for a typical termination (same termination as Figure 2) where a plume impinges on a subducting slab and shuts off subduction.

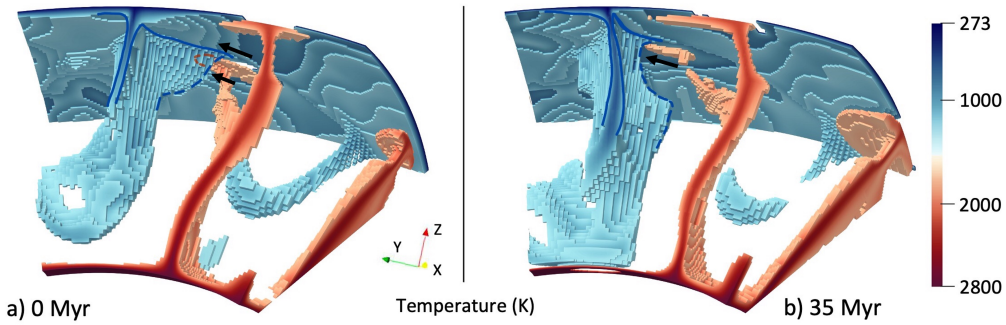

306 **Figure 4.** Annotated version of the time evolution of the second example of termination,
307 Figure 3, where a plume impinges on the side of a subducting slab and shuts off subduction. We
308 have drawn the trench and subducting slab boundaries and included arrows showing motion in
309 the model. Red dashed lines show location of plume behind subducting slab, blue dashed show
310 edges of the subducting slab. Also see movies in Supplementary Information.

311 For Figure 4, we show an interpretation of another style of termination, again we
312 show a small section of the model with the viewpoint in the mantle looking up towards
313 the model surface. This termination occurs when a plume interacts with a subduction
314 zone along its lateral extent. In panel a, we see a plume head sliding into the side of a
315 subducting slab. The plume head is slightly behind the subducting slab edge. As the plume
316 interacts with the slab edge, the slab begins to detach from the surface. In panel b, as
317 the plume continues to slide along the slab, there is an unzipping effect in the subduct-
318 ing slab causing the slab to detach from the surface along the length, ending in a ter-
319 mination. Figure 5 shows the termination in different representations. Here we see in
320 the yield stress (c-d) that the slab is fully weakened and the plume is strong and again
321 in the strain rate (e-f) that the highest values are in the subducting slab near to the sur-
322 face and the mantle plume heads. The total strain (g-h) shows an accumulated strain
323 in the slab of 3-7 with the higher values occurring at the end of the slab, which has ex-
324 perienced the most strain through the subduction but not necessarily where the strain
325 rate is highest.

336 In Figure 6, we show the final style of plume-slab termination discussed here, two
337 plumes pinching out a subduction zone, interpreted in Figure 7. Panel 6a shows the setup
338 of this termination style with a plume on either side of the subducting slab with both
339 plumes moving towards the slab. As the plumes impinge on this subducting slab, a slab

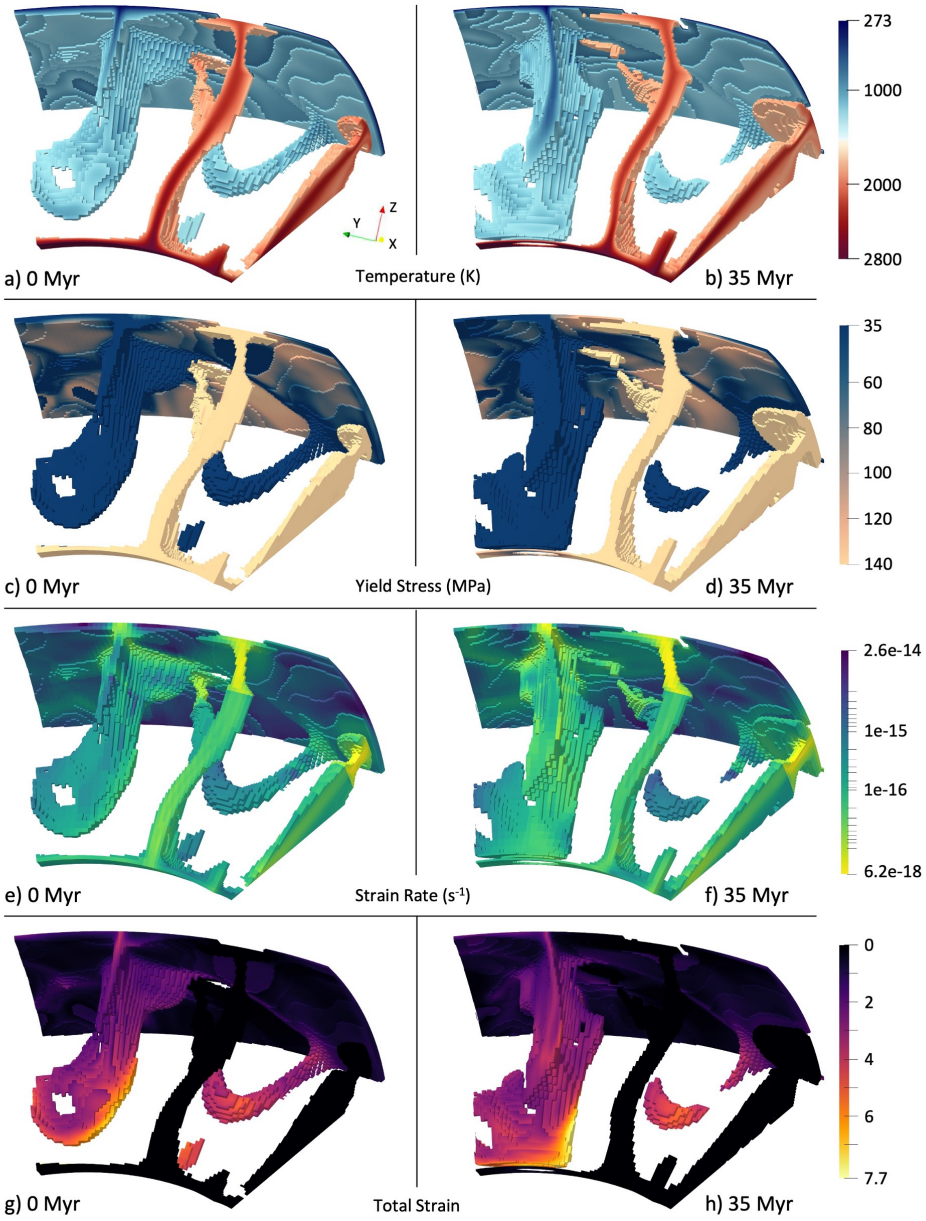

Figure 5. Temperature, yield stress, strain rate, and accumulated strain (damage) before (a, c, e, g) and after termination (b, d, f, h) for a termination where a plume impinges on the edge of a subducting slab and shuts off subduction by unzipping along the slab's length.

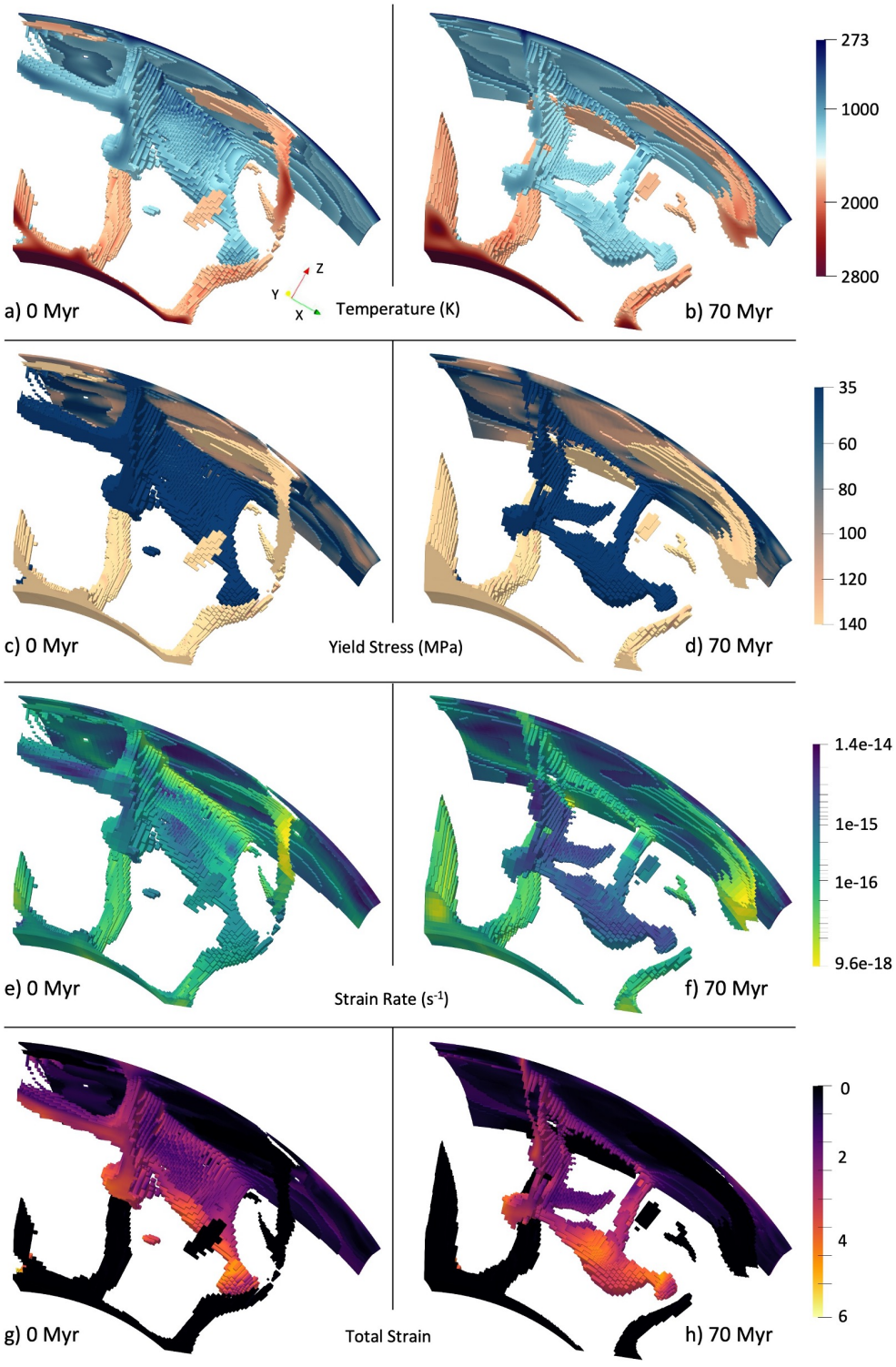

329 **Figure 6.** Temperature, yield stress, strain rate, and accumulated strain (damage) before (a,
330 c, e, g) and after termination (b, d, f, h) for a double-sided termination where two plumes pinch
331 out a subducting slab to shut off subduction.

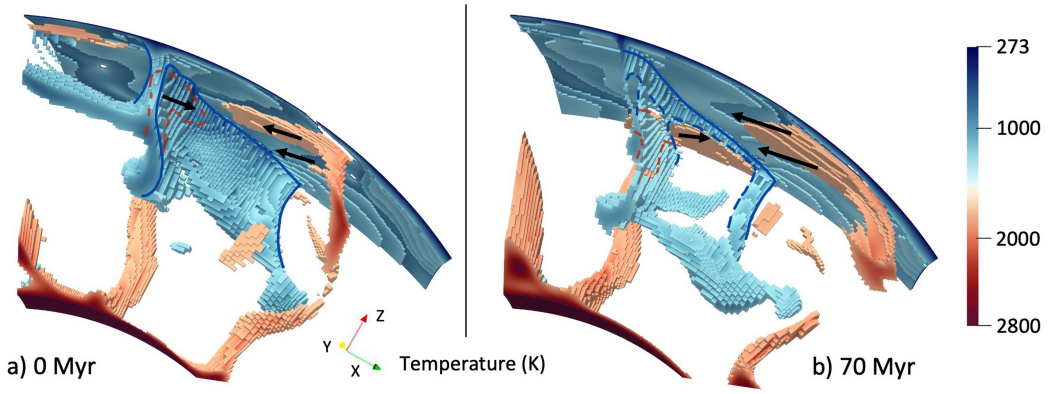

Figure 7. Interpretation of third example of termination where two plumes impinge on either side of a subducting slab leading to termination, Figure 6. We have drawn the trench and subducting slab boundaries and included arrows showing motion in the model. Red dashed lines show location of plume behind subducting slab, blue dashed show edges of the subducting slab.

hole is created in the center of the subducting slab (panel 6b). This slab hole then extends along the length of the subducting zone until the slab is no longer attached to the surface. It is noticeable in this example that the yield stress (6c-d) in the surface is very high surrounding this subduction zone while the subduction zone itself is fully weakened. In the strain rate (6e-f), the near surface bend of the subducting slab has a higher strain rate due to the forces acting on it. In Figure 6g and h, we see the subducting slab has more variable accumulated strain throughout; this can occur due to the rheological differences in the lithosphere that is subducted. As in other terminations, as the detached slab sinks to the CMB the accumulated strain will lessen as the detached slab is heated by the higher temperatures at the CMB.

As may be expected, and explored more fully in 2-D (Heilman & Becker, 2022), not every plume-slab interaction ends in subduction termination. We find at least five instances where a plume interacts with a subducting slab without causing a complete termination, i.e. a roughly 60% chance of plumes shutting down subduction if they get close to slabs, for our chosen parameter values. Some of these plume-slab interactions result in no change to the subducting slab morphology from the plume. In some cases, the plume creates a hole in the subducting slab but subduction is able to continue normally, as has been suggested for modern settings based on seismic tomography.

In our convection models, some subduction margins will obviously cease to operate without the influence of plumes, simply due plate tectonic/convective reorganizations leading to a lack of driving forces, or lack of remaining material to be subducted. In general, convergent margin systems have variable lifespans, between hundreds of millions to a billion years, with individual slab segment lifetimes shorter and controlled by their configuration and evolution. Subduction plate boundary geometries appear somewhat longer-lived and stable without direct impacts from plumes compared to those that experience plumes effects in proximity to the slab, but this is difficult to reliably quantify. Part of the challenge is indeed that slabs and plumes are part of the same mantle convection system. Isolating individual aspects of the dynamics, while helpful for tectonic interpretation, is thus difficult, and to some degree futile for a single model realization, besides the overall impact of plumes that is controlled by internal heating as discussed in sec. 3.3.

3.2 Non-Damage Rheology Model

We also analyzed a model without the damage rheology to compare to the types of plume-slab interactions we observe in the damage model (see Supplementary file S3). In this non-damage model, the background yield stress was lowered to 55 MPa from 140 MPa to achieve the same convective vigor and maintain a mobile convective regime (comparable Rayleigh number of $\sim 3.8 \cdot 10^6$). Yield stress values of order 100 MPa are required to achieve plate-like motions with a mobile lid in our models. Such values are smaller than what would be expected from rock mechanics, a typical finding for visco-plastic, plate-like convection models without (e.g. Moresi & Solomatov, 1998; Tackley, 2000a; van Heck & Tackley, 2008; Foley & Becker, 2009) or with damage (e.g. Tackley, 2000b; Fuchs & Becker, 2019, 2022). This discrepancy in yield stress might indicate some additional weakening mechanism, such as hydration. However, our point here is not about the absolute values, but we merely provide an attempt to compare damage and no-damage cases at similar convective vigor and tectonic style.

Our non-damage model has a total run time of ∼6 overturns, and this model showed only one example of plume-induced subduction termination. In this termination, a plume first formed a hole in a subducting slab, which then caused a slab tear on either side of the slab hole, and lead to the eventual termination of the subduction zone. There were four other instances where a mantle plume caused the formation of a slab hole that did

not result in an immediate termination of subduction. In the non-damage model, the yield stress in the subducting slab is higher on average and not reduced by damage, meaning that strong slabs are less susceptible to plume effects, as expected. This indicates that damage rheology is not required for plume-induced subduction termination, but enhances its frequency, as documented for 2-D (Heilman & Becker, 2022), and implied by the more episodic behavior of tectonics with damage (Landuyt et al., 2008; Foley & Bercovici, 2014; Bercovici & Ricard, 2016; Fuchs & Becker, 2022; Gerya et al., 2021).

3.3 Effect of Internal Heating

We expect the amount of internal heating to affect the importance of plumes, which are trivially absent if there is no bottom heating, and whose effect will be maximal for pure bottom heating. To compare our reference damage rheology results, two other models were run with a lower ($5 \cdot 10^{-13}$ W/kg) and a higher ($2 \cdot 10^{-11}$ W/kg) amount of internal heat production, i.e. 0.1 and 4 times the heat production of the initial damage rheology model. The heat flow time series for the three models are shown in Figure 8. The average heat flow for the reference model (Figure 8a) is 1.81 TW for the CMB and 4.69 TW for the surface. The relative contribution of 61.5% from internal heating for the reference model is in the ballpark of estimates for the Earth's mantle (Leng & Zhong, 2008; Lay et al., 2008; Jaupart et al., 2015), which are uncertain, as noted. The average heat flow for the lower heating model (Figure 8b) is 1.67 TW out of the CMB and 3.77 TW out of the surface, for 55% contribution from internal heating. The average heat flow for the higher heating model (Figure 8c) is 1.76 TW out of the CMB and 7.27 TW out of the surface, for 75% contribution from internal heating.

Considering absolute values, our 3-D spherical chunk is roughly 20% of the surface area of the Earth. Scaling the heat flow out of the surface of the model to Earth would be roughly 23.45 TW for the reference model, and 18.85 TW and 36.35 TW for the lower and higher heating model, respectively. These values are comparable to estimates for the convective heat flow of the mantle, ∼38 TW (Jaupart et al., 2015) and become more favorable when considering that only ∼70% of Earth is covered by oceanic plates. Our focus here is mainly to explore the general controls on plume dynamics, and we did not account for effects such as time-variable heating or secular cooling. However, the overall convective vigor of the models may be comparable to the mantle.

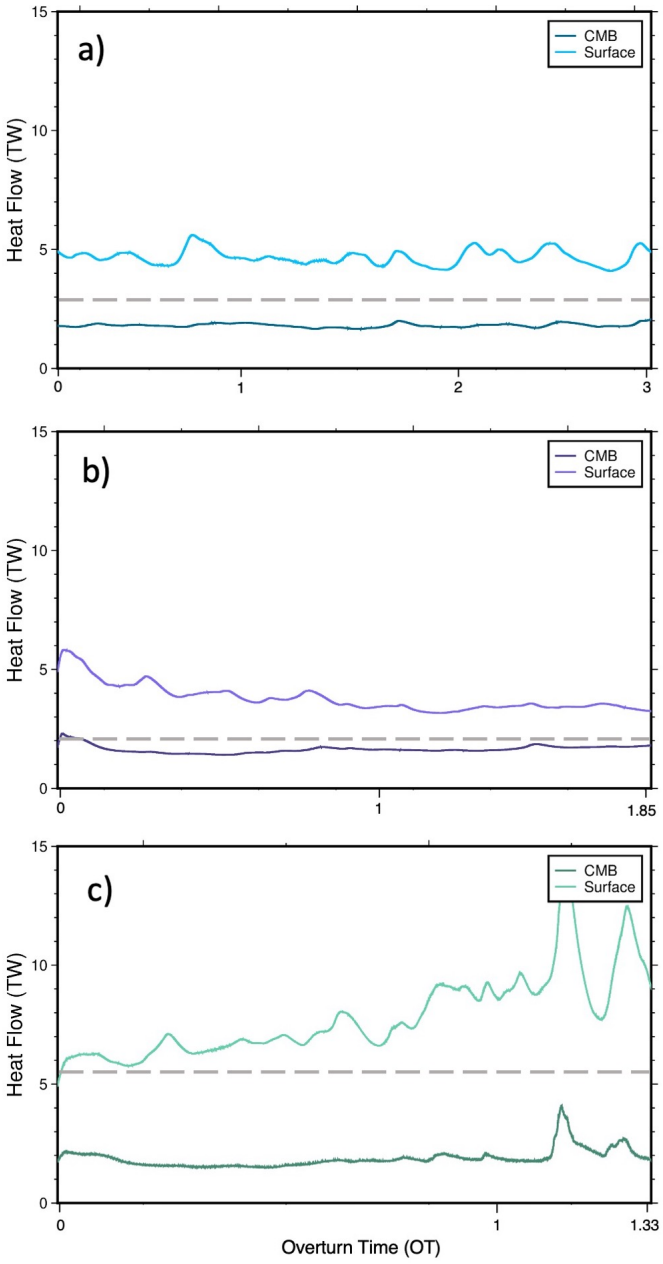

421 **Figure 8.** Heat flow out of the CMB and surface are plotted over overturn times for three
422 models with average internal heating shown as dashed gray line. a) Damage Model. b) Lower
423 Internal Heating Model. c) Higher Internal Heating Model.

Changes of the internal heat production can lead to complexities because different average viscosities result via the temperature-dependent creep laws used, and an interplay with the yield stress controlled tectonic regime. Models do have somewhat different convective vigor, with Rayleigh numbers of $\sim 4.65 \cdot 10^5$, $9.95 \cdot 10^6$, and $7.16 \cdot 10^7$ for the lower, reference, and higher heating cases, respectively, where the Rayleigh number is determined from the temperature difference across the mantle at steady-state in the model run. This has an effect on the planform of convection. However, these models all remain predominantly mobile and in a plate tectonic-like convection regime. Meaning these models should be broadly comparable in terms of their style of dynamics, and frequencies, e.g., of plume-slab interactions comparable through normalized overturn times.

The model with a lower proportion of heating ran for a total of 1.85 overturns from an initial steady state model. This model showed eleven plume-slab terminations, i.e. roughly 5 per overturn. These terminations follow the same trend as in the reference model, where the subducting slab is fully weakened before the termination, strain rate is high in both the slab and plume and lessens after termination, and the subducting slab is damaged prior to termination. We also see in this model a non-termination event creating a slab window in the subducting slab and subduction continues. Specifics of these interactions and the detailed numbers of terminations per a given typical model time are, of course, subject to stochastic fluctuations.

The model with a higher proportion of heating had a total run time of 1.33 overturns after starting from an initial steady state model. This model showed two plume-slab terminations, i.e. $\sim$1.5 terminations per one overturn. This model had hotter average mantle temperatures (2034 K compared to the reference model 1518 K) and therefore hotter subducting slab temperatures due to the increased proportion of internal heating. It was more difficult to identify instances when plumes were actively shutting off subduction as the hotter mantle led to the subducting slabs warming quickly and detaching even without plume influence. The model becomes unstable towards the end of its run time and moves into an episodic regime (as seen in Figure 8c) and may be more relevant for early Earth rather than, say, Cenozoic mantle convection (e.g. van Hunen & van den Berg, 2008; Gerya et al., 2021).

Given variations in the relative importance of bottom and internal heating, we thus find the expected effect on the rate of plume-slab terminations per overturns. All mod-

In press at G-Cubed, June 2024.

els show plume-slab terminations and interactions, but for the lower internal heating model the frequency of plume-termination events was almost double the reference model. The opposite is true for the higher internal heating model with fewer plume driven subduction terminations, substantiating the results of Heilman and Becker (2022). We also ran two other models with intermediate heat production of $8{\cdot}10^{-12}$ W/kg and $1{\cdot}10^{-11}$ W/kg for validation and the termination numbers were in between the higher heat model and the reference model.

Due to the additional degrees of freedom provided by 3-D flow compared to the analysis of Heilman and Becker (2022), and the highly time-dependent nature of the convective system, further, systematic analysis of controlling factors beyond the overall effect of internal heating has to be somewhat limited. We measured internal slab temperature for both terminating and non-terminating plume-slab interactions by sampling temperatures from the subducting slab for a period of 60 Myr (well within the overall termination and interaction times). The temperatures were collected over a 50 km section of the subduction zone where the plume was actively interacting with it, at a spacing of 10 km intervals. These data were averaged over the length (50 km) and the standard deviation was taken to show the variability of temperature within the slab. In general, we find that the non-terminating interactions are typically happening for slabs that are colder and hence thicker, as expected (Heilman & Becker, 2022).

We plot these slab temperatures for terminations and non-terminations as a function of internal heat production (i.e. lower heating model, reference damage model, and higher heating model) in Figure 9. These data points show three terminations, one from each heating model, and three non-terminations, one from each heating model. For these models, the respective average mantle temperatures over the 60 Myr time are 1278, 1518, and 2034 K. As the average mantle temperature increases, plumes contribute less to the convective dynamics, so there are less terminations overall. In Figure 9 we see this reflected in the increase of slab temperature for both termination and non-termination in the highest internal heating scenario over time. In Figure 9c we see that terminations always have higher internal slab temperatures than non-terminations within the same model, regardless of the mantle temperature or internal heating of the model.

In press at G-Cubed, June 2024.

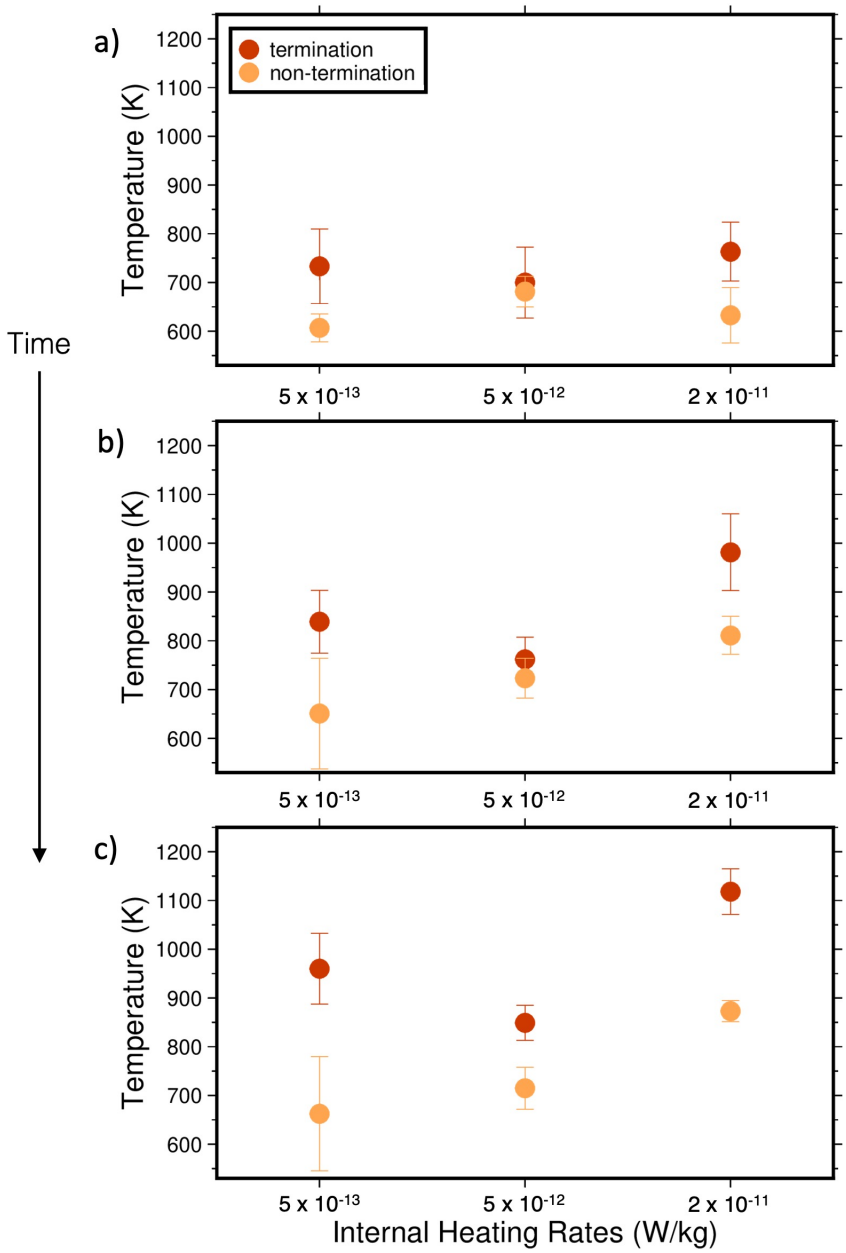

Figure 9. Subducting slab temperatures for terminations and non-terminations for each ratio of internal heating. Plots a), b), and c) increase in 20 Myr time increments showing the trend in slab temperature over time for each internal heating ratio.

4 Discussion

Our models show that plume-driven subduction terminations occur in 3-D spherical geometry convection models, substantiating the suggestion of Heilman and Becker (2022). This implies that plume-induced subduction termination may indeed happen on Earth, if convective vigor and actual rock rheology are similar to those represented by our model.

As our models are freely convecting, rather than being tailored to specific tectonic scenarios, we can only make observations about what sorts of subduction zones get terminated and what the typical geometry and dynamics of those cases are. The main scenarios we observe are a plume head impinging either in front or behind the subducting slab to cause termination (Figures 3 and 5) and plumes on either side of a subducting slab pinching out a subduction zone leading to termination (Figure 6). The first mode of termination is most common in the model, accounting for ∼85% of the terminations in the reference, damage-rheology model, and it is the only mode we observed for the non-damage rheology, lower internal heating, and higher internal heating cases. Typically, this process begins with the plume moving into contact with the subducting slab and then initiating a hole in the subducting slab. In some cases, the plume remains in contact with the subducting slab fully through the termination, or the plume may advect or diffuse away from the subducting slab, but the influx of heat from the plume was enough to cause the termination. The second scenario has two plumes pinching out a subduction zone to cause a termination. We see this type of termination less frequently in our models, and this scenario is perhaps also less likely on Earth as it requires plumes on either side of a subduction zone.

Overall, disruption frequencies were 2.3 terminations/overturn (OT) for the reference model, 0.16 terminations/OT for the non-damage rheology model, 1.85 terminations/OT for the lower heating model, and 1.33 terminations/OT for the higher heating model. With $OT = 300$ Myr, the disruption frequency of terminations is then one termination every ∼50 Myr for the lower heating model, every 130 Myr for the reference model, and every 200 Myr for the higher heating model. Additionally, the non-damage model frequency with its one termination would be every 1.8 billion years. This scaling correlates with the internal heating, as expected (Heilman & Becker, 2022).

In press at G-Cubed, June 2024.

This frequency suggests there are likely several examples of plume-driven subduction termination in Earth's history. Larger total numbers of events are expected given the larger volume of the full spherical shell as compared to our models, at equivalent relative importance, since the latter is controlled to first order by convective vigor. Plume-induced slab terminations are much more likely if slab rheology is not just visco-plastic but if material can be weakened, as is the case for our damage rheology model. While slab pull forces can be supported for plate-like motions even in the presence of weakening (cf. Fuchs & Becker, 2019; Gerya et al., 2021), the accumulated damage makes it easier for the mantle plume to cut through, or pinch out, the subducting slab (Figures 3, 5, and 6). While it is perhaps becoming more broadly accepted that the lithosphere is significantly weakened in the trench region where the plate is bending, our rheological choices may lead to slabs that are weaker than in the Earth's mantle.

Since seafloor, i.e. oceanic lithosphere, age will control slab thickness through half-space cooling, this translates to a preference for slab termination in models or regional tectonic settings where age–area distributions are biased toward younger ages. Our model domain allows for creation of plate geometries that are multiples of the domain depth, with lengths between $\sim 3,000 \ldots 9,000$ km, i.e. aspect ratios between $\sim 1 \ldots 3$. Those are typical ranges for optimizing heat transport in simple convection models, but smaller than some of the largest, and hence oldest, plates that can be realized by global models, or in the case of Earth in the Cenozoic, by the Pacific plate. Given that slab segmentation seems to be ubiquitous (e.g. Tan et al., 2002; Liu & Stegman, 2012; Portner et al., 2020), even if actual slabs are older than in our models on some scales, we expect plume-induced subduction terminations to be less frequent on Earth globally, rather than completely absent. However, we only show oceanic lithosphere in our model and do not consider the relationship with continental lithosphere in these terminations. Plume-modified tectonics will be more pronounced in smaller-scale, younger plate, regional settings such as in the Cordilleran system in the East Pacific, or the Afar-Arabia-Anatolia-Hellenic case.

Resolving what the differences in model geometry and regional plate boundary dynamics imply for our estimates and what plume-slab interactions are expected, is complicated by the fact that age-area distributions for Earth are unlike what boundary layer analysis leads us to expect (e.g. Labrosse & Jaupart, 2007; Becker et al., 2009). Likewise, we cannot simply multiply our estimates of typical occurrence numbers by scal-

ing to the total surface area, since the supercontinental cycle is a strong control on both seafloor age – area distributions (Coltice et al., 2012) and plume distributions (e.g. Jellinek & Manga, 2004; Hassan et al., 2015; Li & Zhong, 2017; Arnould et al., 2020). Hotspots fed by plumes are currently clustered close to the large-low shear wave velocity provinces at the CMB underneath Africa and the Pacific (e.g. Richards et al., 1988; Burke et al., 2008; Boschi et al., 2008; Jackson et al., 2021). Further visco-plastic damage rheology convection modeling, in full 3-D spherical geometries and with a supercontinental cycle, is thus required to resolve the interconnected effects of slab-driven, evolving plate boundaries as modulated by plumes, continental cover, and induced flow.

Besides rheology and variations in tectonics and subduction in a global, thermo-chemical convection system, the other control on the importance of plume-slab interactions is the degree of bottom to internal heating. Our results for a higher to lower rate of internal heating (sec. 3.3 and Figure 9) could be interpreted as being indicative of the evolution of mantle dynamics from the early Earth to present-day. The internal heating of the mantle has decreased by a factor of $\sim$4 over time with an effective timescale of $\sim$3 Ga (e.g. Jaupart et al., 2015) due to the decay of the main radiogenic elements in the mantle. All else being equal, we then expect a greater effect of mantle plumes during the more recent periods of plate tectonics, including relatively more frequent plume-induced subduction terminations. Such effects due to active upwellings may add to the possible contributions of accumulating damage and persistent sutures in the lithosphere to make plate tectonics more time-dependent toward the present, even though the overall convective vigor may decrease with progressive cooling (Foley & Bercovici, 2014; Fuchs & Becker, 2022).

4.1 Comparison to past and modern-day tectonic settings

Plume-slab terminations show interesting dynamics in geodynamic models, but there is also some indication of their existence in past and present-day geology. One example during the Jurassic (201-145 Ma) is related to the Karoo-Ferrar LIP eruption in south-western Gondwana. While it is generally agreed that there was a time of flat slab subduction previous to the LIP emplacement, there is debate as to how this flat slab subduction ended (Dalziel et al., 2000; Luttinen, 2018; Navarrete et al., 2019; Ruhl et al., 2022). Figure 10 shows our interpretation in 3-D of the dynamics of this system, motivated by our model dynamics. If the rising mantle plume was responsible for flat slab

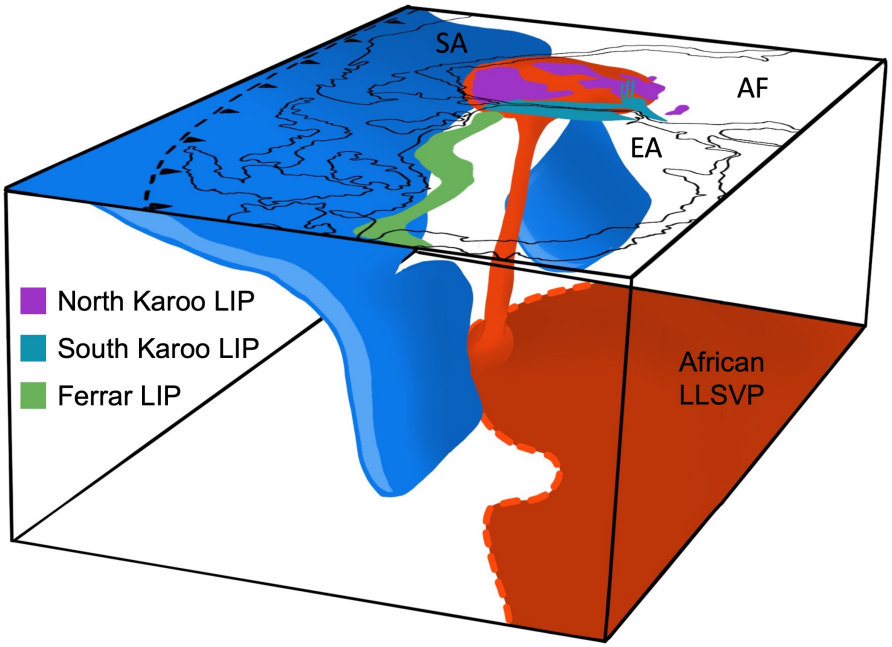

Figure 10. 3-D reconstruction of southwestern Gondwana during the Jurassic showing on the surface the emplacement of LIPs (Luttinen, 2018). Rendering in the mantle shows projected African LLSVP, mantle plume that cutoff subduction underneath southwestern Gondwana and shows propagation of slab shutoff. SA: South America, AF: Africa, and EA: East Antarctica.

subduction (Dalziel et al., 2000), it may have subsequently broke through the slab, reached the lithosphere, and created the Karoo-Ferrar LIP. This scenario can also explain the bilateral geochemical sourcing of the Karoo from both deep mantle sources and subduction-modified upper mantle sources as the plume rises and terminates (Luttinen, 2018). The subducting slab could have then unzipped from where the mantle plume broke through, explaining the subduction-influenced upper mantle signature in the Ferrar LIP (Luttinen, 2018).

A more recent example of plume-slab dynamics is the Arabian-Anatolian-Aegean system (Ershov & Nikishin, 2004; Faccenna et al., 2013; Hua et al., 2023). Subduction in the Mediterranean has been inferred to have been active 30 million years ago as the Afar plume was upwelling under the Arabian plate to the southeast (Faccenna et al., 2019; Straume et al., 2024). Volcanic ages and other constraints have been interpreted such

that the plume then moved northward toward Anatolia, and that this plume advance was driven or at least assisted by mantle flow, including via a fragmentation of the Mediterranean slab. The formation of a slab gap underneath Anatolia leading to the current Hellenic segment of the trench might have led to asthenospheric suction and contributed to Afar plume advance (Faccenna et al., 2013; Straume et al., 2024). Our results here, and the 2-D models of Heilman and Becker (2022), suggest that the Afar plume may have, in fact, played a more active role in partitioning subduction along the northern margin of Africa.

For the modern-day, the Nazca-South American subduction zone may serve as an example for the effect of plumes on slabs. Based on interpretation of seismic tomography, Portner et al. (2017, 2020) suggested that the Juan Fernandez plume, lying west of the trench, was dragged along the bottom of the downgoing slab and rises through the slab by taking advantage of a previously created slab hole. With our model findings, we can speculate that this interaction is the beginning of a plume-slab termination where a slab hole is developed first through plume interaction and a few million years later leads to subduction shutoff. In Figure 11, we interpret the tomography of Portner et al. (2020) for the Nazca slab and mantle with tomography slices every ∼600 km. In this figure the dotted lines are interpretations of the lateral extent of the plume head that has risen through the slab hole and the slab. The mantle plume material that has been dragged by the downgoing slab may have modified and broken through part of the subducting slab. This stage of a plume lying under a subducting slab and creating a slab hole is very similar to the early stages of several terminations that we observe in our model (i.e. Figure 2). In the future, this interaction may turn into a termination if the slab is sufficiently affected by the presence of the plume.

Relevant plume-slab interactions may also be present in other areas for the modern-day, including on the western side of the Pacific where a range of hot anomalies have been imaged in proximity to possibly fragmented slabs (e.g. Obayashi et al., 2009; Tao et al., 2018), and the effects of hot mantle anomalies on subduction have been modeled (e.g. Morishige et al., 2010). Plume-slab interactions in east Asia have been postulated for origin of the Changbaishan volcanic complex, where intraplate volcanism may be driven by a plume disrupting or at least affecting the subducting Pacific plate (Tang et al., 2014). Seismic imaging has been interpreted to show hot material from the deep mantle rising through a gap in the subducting slab at depth (Tang et al., 2014), a type of interaction

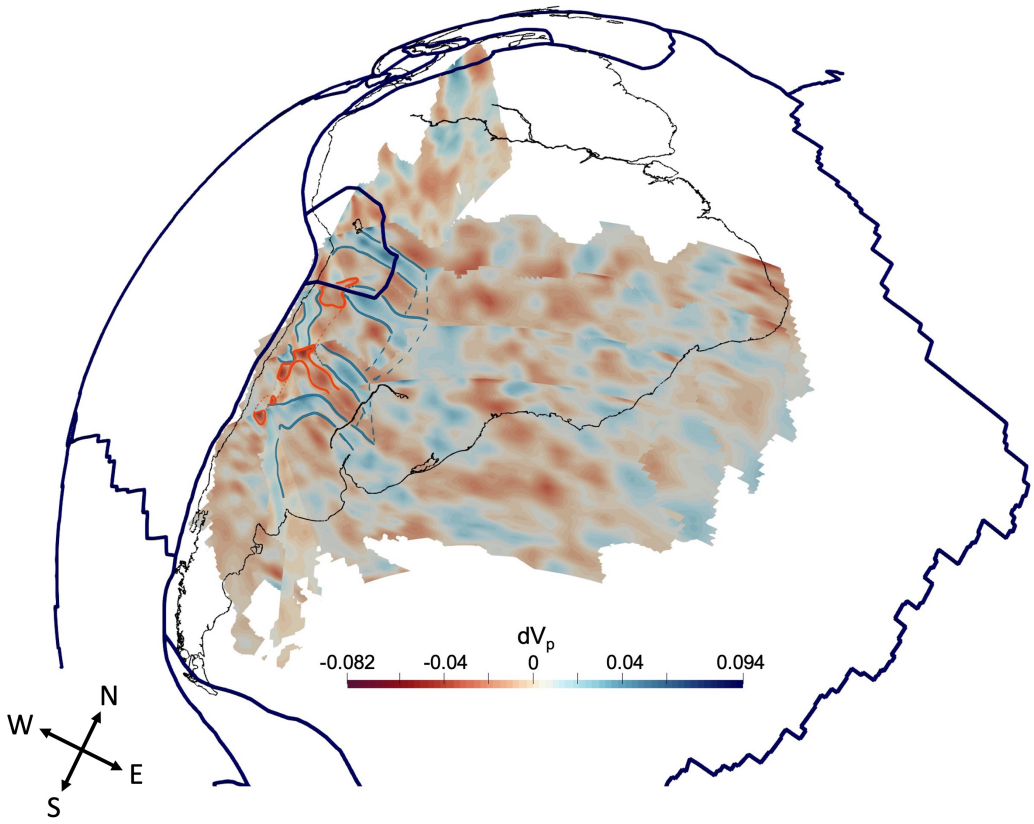

Figure 11. Tomography fence diagram of southern South America using dV_p using tomographic data from Portner et al. (2020). Interpretation of 3D plume-slab interaction structure is overlain in blue for subducting slab and red for mantle plume head. South America is outlined in black while tectonic plates are outlined in dark blue and the trench of the subduction zone is the dark blue line directly to the west of South America.

between plumes and slabs consistent with our model findings. While this setting shows a promising interaction between a plume and subducting slab, it is likely not leading to a termination as the rising plume interacts with the slab at a depth of 660 km or greater. Our models find terminations likely when the plume-slab interaction occurs near the lithosphere. However, this example gives confidence to the feasibility of mantle plumes modifying and creating slab holes in subducting slabs.

5 Conclusions

We find that plume-induced subduction termination occurs in 3-D, spherical geometry mantle convection models. Terminations are found throughout our models, but are more likely in cases with damage rheology. A single plume can directly shut off subduction by puncturing and cutting off a slab from below, two plumes can pinch out subduction from the side, and a single plume can cause an lateral unzipping of a descending slab. Natural examples where these processes may help explain the thermo-chemical evolution of the continental lithosphere include the Karoo-Ferrar LIP, the Afar-Anatolia Aegean system, and present-day settings in the western and eastern Pacific subduction systems. Plume-slab termination frequency is inversely related to the proportion of internal heating, implying that plume-slab interactions may have become more prevalent over planetary evolution. Our models can contribute to a better understanding of the relationship between subducting slabs and rising mantle plumes and the effect and expressions of slab-plume "talk-back" in the evolution of the plate tectonic system.

6 Open Research

ASPECT is an open-source mantle convection code hosted by the Computational Infrastructure for Geodynamics, all features used are available in ASPECT version 2.4.0-pre (Bangerth et al., 2022). The necessary parameter files to replicate models can be found at (Heilman, 2023).

Acknowledgments

We thank the editor, associate editor, and reviewers for their helpful suggestions, and J. Dannberg and C. Faccenna for comments on an earlier thesis chapter. This project was funded by the National Science Foundation under award EAR-1853856. We also thank the developers and the Computational Infrastructure for Geodynamics (geodynamics.org)

which is funded by the National Science Foundation under award EAR-0949446 and EAR-1550901 for supporting the development of ASPECT, and Portner et al. (2020) for making their tomographic model available freely.

References

Arnould, M., Coltice, N., Flament, N., & Mallard, C. (2020). Plate tectonics and mantle controls on plume dynamics. *Earth Planet. Sci. Lett.*, *547*, 116439.

Auth, C., Bercovici, D., & Christensen, U. R. (2003). Two-dimensional convection with a self-lubricating, simple-damage rheology. *Geophys. J. Int.*, *154*, 783–800.

Baes, M., Sobolev, S., Gerya, T., & Brune, S. (2020). Plume-induced subduction initiation: Single-slab or multi-slab subduction? *Geochem., Geophys., Geosys.*, *21*(2), e2019GC008663.

Bangerth, W., Dannberg, J., Fraters, M., Gassmoeller, R., Glerum, A., Heister, T., ... Naliboff, J. (2022, July). *Aspect v2.4.0 [software].* Zenodo. Retrieved from `https://doi.org/10.5281/zenodo.6903424` doi: 10.5281/zenodo.6903424

Becker, T. W., Conrad, C. P., Buffett, B., & Müller, R. D. (2009). Past and present seafloor age distributions and the temporal evolution of plate tectonic heat transport. *Earth Planet. Sci. Lett.*, *278*, 233–242.

Bercovici, D., & Ricard, Y. (2016). Grain-damage hysteresis and plate tectonic states. *Phys. Earth Planet. Inter.*, *253*, 31–47.

Betts, P. G., Mason, W. G., & Moresi, L. (2012). The influence of a mantle plume head on the dynamics of a retreating subduction zone. *Geology*, *40*(8), 739-742.

Boschi, L., Becker, T. W., & Steinberger, B. (2008). On the statistical significance of correlations between synthetic mantle plumes and tomographic models. *Phys. Earth Planet. Inter.*, *167*, 230–238.

Burke, K., Steinberger, B., Torsvik, T. H., & Smethurst, M. A. (2008). Plume generation zones at the margins of large low shear velocity provinces on the core-mantle boundary. *Earth Planet. Sci. Lett.*, *265*, 49–60.

Coltice, N., Rolf, T., Tackley, P. J., & Labrosse, S. (2012). Dynamic causes of the relation between area and age of the ocean floor. *Science*, *336*, 335–338.

Dalziel, I. W., Lawver, L., & Murphy, J. (2000). Plumes, orogenesis, and superconti-

nental fragmentation. *Earth and Planetary Science Letters*, *178*(1-2), 1–11.

Dannberg, J., & Gassmöller, R. (2018). Chemical trends in ocean islands explained by plume–slab interaction. *Pro. Nat. Acad. Sci.*, *115*, 4351–4356.

Davies, G. F. (1986). Mantle convection under simulated plates: effects of heating modes and ridge and trench migration, and implications for the core-mantle boundary, bathymetry, the geoid and Benioff zones. *Geophys. J. R. Astr. Soc.*, *84*, 153–183.

Druken, K., Kincaid, C., Griffiths, R., Stegman, D., & Hart, S. (2014). Plume–slab interaction: the Samoa–Tonga system. *Phys. Earth Planet. Inter.*, *232*, 1–14.

Duggen, S., Hoernle, K., Hauff, F., Klügel, A., Bouabdellah, M., & Thirlwall, M. F. (2009). Flow of Canary mantle plume material through a subcontinental lithospheric corridor beneath Africa to the Mediterranean. *Geology*, *37*, 283—286.

Enns, A., Becker, T. W., & Schmeling, H. (2005). The dynamics of subduction and trench migration for viscosity stratification. *Geophys. J. Int.*, *160*, 761–775.

Ershov, A., & Nikishin, A. (2004). Recent geodynamics of the Caucasus-Arabia-east Africa region. *Geotectonics*, *38*, 123–136.

Faccenna, C., Becker, T. W., Jolivet, L., & Keskin, M. (2013). Mantle convection in the Middle East: Reconciling Afar upwelling, Arabia indentation and Aegean trench rollback. *Earth Planet. Sci. Lett.*, *375*, 254–269.

Faccenna, C., Glišović, P., Forte, A., Becker, T. W., Garzanti, E., Sembroni, A., & Gvirtzman, Z. (2019). Role of dynamic topography in sustaining the Nile River over 30 million years. *Nature Geosc.*, *12*, 1012–1017.

Fletcher, M., & Wyman, D. A. (2015). Mantle plume-subduction zone interactions over the past 60 Ma. *Lithos*, *233*, 162-173.

Foley, B. J., & Becker, T. W. (2009). Generation of plate tectonics and mantle heterogeneity from a spherical, visco-plastic convection model. *Geochem., Geophys., Geosys.*, *10*(Q08001). doi: 10.1029/2009GC002378

Foley, B. J., & Bercovici, D. (2014). Scaling laws for convection with temperature-dependent viscosity and grain-damage. *Geophys. J. Int.*, *199*, 580–603.

Fraters, M. R. T., Bangerth, W., Thieulot, C., Glerum, A. C., & Spakman, W. (2019). Efficient and practical Newton solvers for nonlinear Stokes systems in geodynamics problems. *Geophys. J. Int.*, *218*, 873–894.

Fuchs, L., & Becker, T. W. (2019). Role of strain-dependent weakening memory on

the style of mantle convection and plate boundary stability. *Geophys. J. Int.*, *218*, 601–618.

Fuchs, L., & Becker, T. W. (2021). Deformation memory in the lithosphere: A comparison of damage-dependent weakening and grain-size sensitive rheologies. *J. Geophys. Res.*, *126*, e2020JB020335.

Fuchs, L., & Becker, T. W. (2022). On the role of rheological memory for convection-driven plate reorganizations. *Geophys. Res. Lett.*, *49*, e2022GL099574.

Gerya, T. V., Bercovici, D., & Becker, T. (2021). Dynamic slab segmentation due to brittle-ductile damage in the outer rise. *Nature*, *599*, 245–250.

Gerya, T. V., Stern, R. J., Baes, M., Sobolev, S. V., & Whattam, S. A. (2015). Plate tectonics on the Earth triggered by plume-induced subduction initiation. *Nature*, *527*(7577), 221–225.

Glerum, A., Thieulot, C., Fraters, M., Blom, C., & Spakman, W. (2018). Nonlinear viscoplasticity in ASPECT: benchmarking and applications to subduction. *Solid Earth*, *9*, 267–294.

Hager, B. H. (1984). Subducted slabs and the geoid: constraints on mantle rheology and flow. *J. Geophys. Res.*, *89*, 6003–6015.

Hassan, R., Flament, N., Gurnis, M., Bower, D. J., & Müller, D. (2015). Provenance of plumes in global convection models. *Geochem., Geophys., Geosys.*, *16*, 1465–1489.

Heilman, E. (2023). *Parameter files for convection model runs [dataset].* Retrieved from `https://doi.org/10.5281/zenodo.8102543` doi: 10.5281/zenodo.8102543

Heilman, E., & Becker, T. W. (2022). Plume-slab interactions can shut off subduction. *Geophysical Research Letters*, *49*, e2022GL099286.

Heister, T., Dannberg, J., Gassmöller, R., & Bangerth, W. (2017). High accuracy mantle convection simulation through modern numerical methods – II: realistic models and problems. *Geophys. J. Int.*, *210*, 833–851.

Hua, J., Fischer, K., Gazel, E., Parmentier, E., & Hirth, G. (2023). Long-distance asthenospheric transport of plume-influenced mantle from Afar to Anatolia. *Geochem., Geophys., Geosys.*, *24*, e2022GC010605.

Jackson, M. G., Becker, T. W., & Steinberger, B. (2021). Spatial characteristics

of recycled and primordial reservoirs in the deep mantle. *Geochem., Geophys., Geosys.*, *22*, e2020GC009525.

Jaupart, C., Labrosse, S., Lucazeau, F., & Marechal, J.-C. (2015). Temperatures, heat and energy in the mantle of the Earth. In G. Schubert (Ed.), *Treatise on geophysics* (2nd ed., pp. 223–270). Elsevier.

Jellinek, A. M., & Manga, M. (2004). Links between long-lived hot spots, mantle plumes, D", and plate tectonics. *Rev. Geophys.*, *42*(RG3002). doi: 10.1029/2003RG000144

Kincaid, C., Druken, K., Griffiths, R. W., & Stegman, D. R. (2013). Bifurcation of the Yellowstone plume driven by subduction-induced mantle flow. *Nature Geosc.*, *6*, 395–399.

Koppers, A. A., Becker, T. W., Jackson, M. G., Konrad, K., Müller, R. D., Romanowicz, B., ... Whittaker, J. M. (2021). Mantle plumes and their role in earth processes. *Nature Rev. Earth & Environ.*, *2*, 382–401.

Kronbichler, M., Heister, T., & Bangerth, W. (2012). High accuracy mantle convection simulation through modern numerical methods. *Geophys. J. Int.*, *191*, 12–29.

Labrosse, S., & Jaupart, C. (2007). Thermal evolution of the Earth: Secular changes and fluctuations of plate characteristics. *Earth Planet. Sci. Lett.*, *260*, 465–481.

Landuyt, W., & Bercovici, D. (2009). Formation and structure of lithospheric shear zones with damage. *Phys. Earth Planet. Inter.*, *175*(115–126).

Landuyt, W., Bercovici, D., & Ricard, Y. (2008). Plate generation and two-phase damage theory in a model of mantle convection. *Geophys. J. Int.*, *174*, 1065–1080.

Lavier, L. L., Buck, W. R., & Poliakov, A. N. B. (2000). Factors controlling normal fault offset in an ideal brittle layer. *J. Geophys. Res.*, *105*, 23431—23442.

Lay, T., Hernlund, J., & Buffett, B. (2008). Core-mantle boundary heat flow. *Nature Geosc.*, *1*, 25–32.

Leng, W., & Zhong, S. (2008). Controls on plume heat flux and plume excess temperature. *J. Geophys. Res.*, *113*.

Li, M., & Zhong, S. (2017). The source location of mantle plumes from 3D spherical models of mantle convection. *Earth Planet. Sci. Lett.*, *478*, 47–57.

Liu, L., & Stegman, D. R. (2012). Origin of Columbia River flood basalt controlled by propagating rupture of the Farallon slab. *Nature*, *482*, 386–389.

Luttinen, A. V. (2018). Bilateral geochemical asymmetry in the Karoo Large Igneous Province. *Scientific Reports*, *8*, 5223.

Mériaux, C., Duarte, J. C., Schellart, W. P., & Mériaux, A.-S. (2015). A two-way interaction between the Hainan plume and the Manila subduction zone. *Geophys. Res. Lett.*, *42*, 5796–5802. doi: 10.1002/2015GL064313

Moresi, L. N., & Solomatov, V. (1998). Mantle convection with a brittle lithosphere: thoughts on the global tectonic styles of the Earth and Venus. *Geophys. J. Int.*, *133*, 669–682.

Morishige, M., Honda, S., & Yoshida, M. (2010). Possibility of hot anomaly in the sub-slab mantle as an origin of low seismic velocity anomaly under the subducting Pacific plate. *Phys. Earth Planet. Inter.*, *183*, 353–365.

Navarrete, C., Gianni, G., Encinas, A., Márquez, M., Kamerbeek, Y., Valle, M., & Folguera, A. (2019). Triassic to Middle Jurassic geodynamic evolution of southwestern Gondwana: From a large flat-slab to mantle plume suction in a rollback subduction setting. *Earth-Science Reviews*, *194*, 125–159.

Obayashi, M., Yoshimitsu, J., & Fukao, Y. (2009). Tearing of stagnant slab. *Science*, *324*, 1173–1175.

Obrebski, M., Allen, R. M., Xue, M., & Hung, S.-H. (2010). Slab-plume interaction beneath the Pacific Northwest. *Geophys. Res. Lett.*, *37*(L14305). doi: 10.1029/2010GL043489

Ogawa, M. (2003). Plate-like regime of a numerically modeled thermal convection in a fluid with temperature-, pressure-, andstress-history-dependent viscosity. *J. Geophys. Res.*, *108*(B2), 2067. doi: 10.1029/2000JB000069

Portner, D. E., Beck, S., Zandt, G., & Scire, A. (2017). The nature of subslab slow velocity anomalies beneath south america. *Geophys. Res. Lett.*, *44*(10), 4747-4755.

Portner, D. E., Rodríguez, E. E., Beck, S., Zandt, G., Scire, A., Rocha, M. P., ... others (2020). Detailed structure of the subducted nazca slab into the lower mantle derived from continent-scale teleseismic p wave tomography. *Journal of Geophysical Research: Solid Earth*, *125*(5), e2019JB017884.

Pusok, A. E., & Stegman, D. R. (2020). The convergence history of India-

Eurasia records multiple subduction dynamics processes. *Science adv.*, *6*(19), eaaz8681.

Rey, P. F., Coltice, N., & Flament, N. (2014). Spreading continents kick-started plate tectonics. *Nature*, *513*, 405–408.

Ricard, Y., Richards, M. A., Lithgow-Bertelloni, C., & Le Stunff, Y. (1993). A geodynamic model of mantle density heterogeneity. *J. Geophys. Res.*, *98*, 21895–21909.

Richards, M. A., Hager, B. H., & Sleep, N. H. (1988). Dynamically supported geoid highs over hotspots: Observation and theory. *J. Geophys. Res.*, *93*, 7690–7708.

Ruhl, M., Hesselbo, S. P., Jenkyns, H. C., Xu, W., Silva, R. L., Matthews, K. J., ... Riding, J. B. (2022). Reduced plate motion controlled timing of Early Jurassic Karoo-Ferrar large igneous province volcanism. *Science Advances*, *8*, eabo0866.

Stein, C., & Hansen, U. (2013). Arrhenius rheology versus Frank-Kamenetskii rheology–Implications for mantle dynamics. *Geochem., Geophys., Geosys.*, *14*, 2757–2770. doi: 10.1002/ggge.20158

Steinberger, B., & Calderwood, A. (2006). Models of large-scale viscous flow in the Earth's mantle with constraints from mineral physics and surface observations. *Geophys. J. Int.*, *167*, 1461–1481.

Straume, E. O., Steinberger, B., Becker, T. W., & Faccenna, C. (2024). Impact of mantle convection and dynamic topography on the Cenozoic paleogeography of Central Eurasia and the West Siberian Seaway. *Earth Planet. Sci. Lett.*, *630*, 118615.

Sun, D., Miller, M. S., Holt, A. F., & Becker, T. W. (2014). Hot upwelling conduit beneath the Atlas Mountains, Morocco. *Geophys. Res. Lett.*, *41*, 8037–8044. doi: 10.1002/2014GL061884

Tackley, P. J. (2000a). Self-consistent generation of tectonic plates in time-dependent, three-dimensional mantle convection simulations 1. Pseudoplastic yielding. *Geochem., Geophys., Geosys.*, *1*(1021). doi: 10.1029/2000GC000036

Tackley, P. J. (2000b). Self-consistent generation of tectonic plates in time-dependent, three-dimensional mantle convection simulations 2. Strain weakening and asthenosphere. *Geochem., Geophys., Geosys.*, *1*(1026). doi:

10.1029/2000GC000043

Tan, E., Gurnis, M., & Han, L. (2002). Slabs in the lower mantle and their modulation of plume formation. *Geochem., Geophys., Geosys.*, *3*(1067). doi: 10.1029/2001GC000238

Tang, Y., Obayashi, M., Niu, F., Grand, S. P., Chen, Y. J., Kawakatsu, H., ... Ni, J. F. (2014). Changbaishan volcanism in northeast China linked to subduction-induced mantle upwelling. *Nature Geoscience*, *7*, 470–475.

Tao, K., Grand, S. P., & Niu, F. (2018). Seismic structure of the upper mantle beneath Eastern Asia from full waveform seismic tomography. *Geochem., Geophys., Geosys.*, *19*, 2732–2763.

Ueda, K., Gerya, T., & Sobolev, S. V. (2008). Subduction initiation by thermal–chemical plumes: numerical studies. *Phys. Earth Planet. Inter.*, *171*, 296–312.

van Heck, H., & Tackley, P. J. (2008). Planforms of self-consistently generated plate tectonics in 3-D spherical geometry. *Geophys. Res. Lett.*, *35*(L19312). doi: 10.1029/2008GL035190

van Hinsbergen, D. J. J., Steinberger, B., Doubrovine, P., & Gassmöller, R. (2011). Acceleration-deceleration cycles of India-Asia convergence: roles of mantle plumes and continental collision. *J. Geophys. Res.*, *116*(B06101). doi: 10.1029/2010JB008051

van Hinsbergen, D. J. J., Steinberger, B., Guilmette, C., Maffione, M., Gürer, D., Peters, K., ... others (2021). A record of plume-induced plate rotation triggering subduction initiation. , *14*, 626–630.

van Hunen, J., & van den Berg, A. P. (2008). Plate tectonics on the early Earth: limitations imposed by strength and buoyancy of subducted lithosphere. *Lithos*, *103*, 217-235.

Zhong, S. (2006). Constraints on thermochemical convection of the mantle from plume heat flux, plume excess temperature and upper mantle temperature. *J. Geophys. Res.*, *111*. doi: 10.1029/2005JB003972